11

Feasibility of a Planet Finder Mission

INTRODUCTION

The preceding chapters of this report provide the scientific rationale for the development of a space-based, variable-baseline infrared interferometer for investigations of extrasolar planets and general astrophysics. The most direct way to demonstrate feasibility of TPF is by taking the science requirements laid out in the preceding chapters and developing a complete mission that satisfies those requirements. Thus, we can be sure that the full set of systems necessary to build TPF has been identified. Such a reference mission, along with its more challenging aspects and approaches to their solution, is described in this chapter. Specific technologies required by this mission and programs for their development are detailed in Chapter 12. Although further project studies will be necessary for detailed mission design and optimization, the studies described below indicate that the development and implementation of a Terrestrial Planet Finder mission is indeed possible within the next decade.

Earlier studies (ExNPS Report 1996) identified a two-by-two matrix of top-level mission designs: separated-spacecraft vs. single-structure and orbiting the sun at 1 AU vs. 5 AU. The benefits and drawbacks of each of these mission classes are summarized in Table 11.1. In December 1997, three industrial contractors (Ball, Lockheed Martin, and TRW) presented reports to JPL in which they explored trades between the 1 AU and 5 AU options for TPF, with emphasis on a single-spacecraft mission. A tethered-spacecraft option was also considered, but was determined to be more expensive and higher risk, due to increased complexity, than the other two spacecraft options. At the same time, the Massachusetts Institute of Technology (MIT) presented an early-phase trade study, focused on system mass, of single- and separated-spacecraft designs (Stephenson 1998).

The TPF science working group determined shortly afterward that the greatest scientific return would be provided by a separated-spacecraft mission operating at 1 AU. Foremost among the benefits offered by the separated spacecraft option is the ability to perform the milli-arcsecond resolution imaging described in Chapter 8; a single structure would seriously limit the possible resolution and the *uv*-plane coverage. The ability to vary the system baseline over a wide range will also

Table 11.1. Trade Matrix

	Advantages	Disadvantages
Separated Spacecraft	• Tunable baseline for planet finding. • Astrophysics imaging capability. • Provides heritage for future separated missions. • Less structural mass. • Multiple launch is possible.	• Multiple spacecraft buses and avionics systems. • Requires development of formation flying systems. • Potential for neighboring spacecraft to cause contamination. • More propellant mass.
Single Spacecraft	• Single set of spacecraft subsystems. • Less propellant mass.	• Complex, high-risk deployment. • More structural mass. • Attitude and jitter control for large structure.
1 AU	• Large amounts of available solar power. • Multiple passes over each part of sky (1-year orbit period). • Easier communications. • Larger launch capacity or multiple launch possible.	• Passive cooling harder. • Increased zodiacal dust. • Larger apertures required.
5 AU	• Smaller collectors needed (therefore available sooner). • Less zodiacal dust. • Passive cooling easier.	• Long delay between launch and arrival on station. • Less power available. • More difficult communications. • 11-year orbit period. • More autonomy required.

improve TPF's capabilities for planet searching, as indicated by Figure 7.4, enabling observation of M stars and a larger population of K stars. The advances in large cryogenic optics resulting from NGST enable the 1 AU mission to match the signal-to-noise of the previously studied 5 AU mission while simplifying many aspects of the mission design, particularly power systems. The 1 AU orbit also decreases the orbital period, providing multiple opportunities to view each target over the lifetime of the mission, and drastically reduces the time required for TPF to reach its operational orbit and begin taking science data.

Later studies at JPL, along with the earlier contractor studies showed no significant cost difference between the two spacecraft options. As a result of these studies and the increased scientific benefits, the 1 AU separated-spacecraft mission was chosen for more detailed study. In August 1998, a team composed of the three industrial contractors and JPL began a study to investigate the feasibility of this preferred mission,

using the prior studies as a starting point. Each contractor investigated a different broadly defined element of the mission design, with JPL staff supplying additional expertise in several areas. The mission described in this chapter is the result of that collaboration.

The interferometer is the main driver of the TPF mission requirements and will be described first. There are many possible choices of beam combiner configuration, some of which are discussed in Chapter 6, but the optical systems involved in building the TPF interferometer (for both nulling and imaging) are substantially the same for all configurations. These systems and their requirements are detailed in the TPF instrument section.

The complete space mission and the subsystems necessary to implement the TPF interferometer as a variable-baseline, separated-spacecraft instrument are discussed in the next section. Many of the system elements are already well understood and the TPF requirements can be satisfied by existing technologies and design techniques. Such systems will be described briefly for completeness, but little detail will be provided. Several aspects, listed in Table 11.2, will require substantial TPF-specific study before implementation, but can be realistically addressed in the design and development phases of the mission. These issues and approaches to their resolution are addressed in detail following the general mission description. In some cases, such as thermal design for passive cooling and system packaging and deployment, preliminary solutions that satisfy TPF requirements are presented. Additionally, some of these issues will be resolved well before Phase A through the development of appropriate technologies for other missions as described in Chapter 12.

THE TPF INSTRUMENT

The TPF interferometer can be configured in several ways, although the limited number of available telescopes requires a performance tradeoff between the ability to provide a deep and wide null to suppress starlight and the ability to chop to suppress large-scale diffuse emission from a zodiacal cloud. Although this limitation would exist with any one configuration, it may be possible to design TPF with the ability to reconfigure its beam-combining optics through an exchange of

Table 11.2. Principal Mission Development Issues

TPF Instrument (nulling)
Formation Flying
Thermal Design for Passive Cooling
Contamination of Thermal and Optical Surfaces
Orbit Selection
Launch Vehicle Packing and System Deployment
Integration and Test

combiner modules. With four telescopes in a linear array, there are a number of possible beam combinations: the null depth can vary as field angle, θ^2, θ^4, or θ^6, depending on how the light is divided and combined from each telescope, as outlined in Table 6.2. The instrument could then be configured to optimize the array for each target source.

The depth and stability of the starlight null drive the system requirements. The depth of the null is degraded by a number of factors: residual wavefront aberrations, beam shear, amplitude mismatch between beams, vibrations, errors in telescope pointing, polarization mismatch in the paths of each beam, stray light, and smearing due to the wavelength dependence of the fringe pattern. A deep and stable null is required so that performance is dominated by noise from local and exo-zodiacal light.

In the following, we consider details of light collection, transport, beam combination, and other systems that will be necessary in any implementation of TPF. A four-element linear array is considered as the baseline to provide a consistent reference for describing the system elements. The precise configuration of the TPF mission will depend greatly on knowledge gained from experience with stellar interferometers presently in development.

ARRAY CONFIGURATION

The TPF instrument consists of the optics, mounts, and associated actuators, all of which are passively cooled to less than 40 K, as well as the colder, actively-cooled detection system. The instrument is distributed among the five modules represented by the four telescopes and the separate beam combiner, illustrated in Figure 11.1. In operational configuration, all these elements are co-planar. The wavefronts sampled by telescopes in the array must arrive at the beam combiner with near-zero relative delay if interference fringes are to be detected. Figure 11.1 illustrates how the beams can be relayed between the collector spacecraft to adjust the pathlengths. The collectors are equally spaced along the interferometer baseline, and the combiner is located at the vertex of an isosceles triangle formed with the two inner collectors. The pathlengths are equalized by relaying the light from each of the four collectors, first to the nearest inner collector, and then to the beam combiner. For the two inner collectors, the light first travels to the opposite inner collector before being relayed to the beam combiner. This arrangement minimizes polarization effects by employing small and equal incidence angles that are balanced in each light path. Pathlength drifts between spacecraft are controlled using signals from lasers and accelerometers.

COLLECTOR TELESCOPES

The science requirement specifies primary mirrors with a 3.5 m diameter, or equivalent collecting area, to guarantee that the planet signal can be detected above noise from background sources, including the

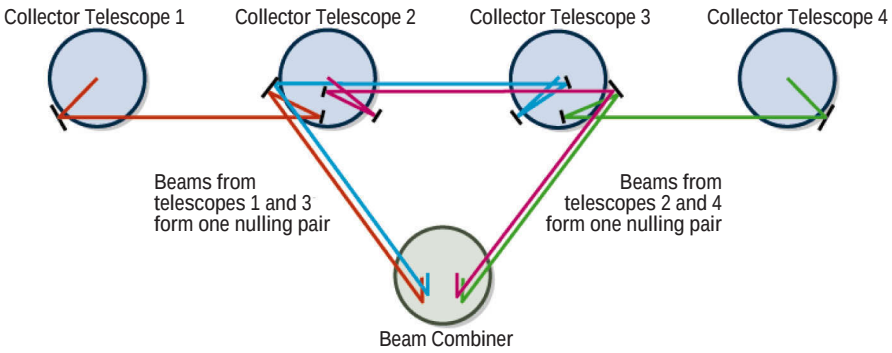

Figure 11.1. Array geometry showing optical paths to the combiner.

local zodiacal light, exo-zodiacal light, and star leakage through the on-axis null.

The fringe contrast necessary to suppress the signal from the star requires that the sum of all wavefront errors introduced by the optics prior to the beam combiner be less than ~100 nm rms. This will provide a 67.4% Strehl ratio at 1 µm, 92.2% at 2.2 µm, and 99.6% at 10 µm, and the required null depth after spatial filtering. This requirement imposes a constraint on the surface-figure quality of the optics and sets a limit on the size of the wavefront errors introduced as the beams propagate from the collector telescopes to the combiner.

When a beam travels from the telescope to the beam combiner, the shape and amplitude distribution of the wavefront will change as the beam diffracts and expands. The effects of beam propagation degrade the interference null, but can be reduced by the use of oversize optics and control of beam shear and parallelism. Diffraction can be studied by analyzing the optical instrument with an analysis code that has near-field diffraction capability.

The effects of stray light must also be addressed. Ideally, a pixel on the detector would look back through the optical train and see only the cold background sky and cold instrument surfaces whose thermal emission is small compared to the signal from the target. Sources of straylight and thermal emission can be identified by analyzing the instrument with commercial straylight-analysis codes such as APART and optical analysis codes such as Modelling and Analysis for Controlled Optical Systems (MACOS), and will be controlled using cold pupil stops, field stops, and baffles.

Two prototype designs for the TPF telescopes have been studied. A schematic representation of the first of these designs, a five-mirror Coudé-folded Ritchey-Chrétien telescope, is shown in Figure 11.2. To minimize off-axis aberrations, fine guidance sensors are used to keep the telescopes pointed to within approximately one arcsecond of the target star, using alignment struts with cryogenic actuators. A fifth mirror, which is a steerable flat, directs the ~15 cm diameter colli-

mated beam toward a relay mirror on one of the adjacent collector spacecraft. Stray-light from radiation sources outside the field-of-view of the telescopes is blocked with a field stop at the focus of the primary-secondary system and a pupil stop in the collimated beam before the steering mirror. A laser beacon from the combiner spacecraft provides a system boresight, and a quad-cell-based detector is used to close the control loops that keep the relay and steering mirrors pointed accurately. Another candidate design has similar control loops, although it is based on a three-element Gregorian configuration and uses a steerable flat for the third element to direct the outgoing collimated beam.

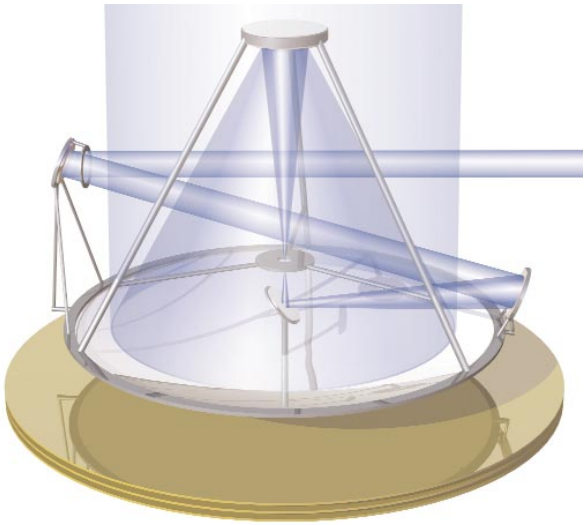

Figure 11.2. Collector optics schematic showing a possible arrangement of beam transfer and steering mirrors.

CENTRAL BEAM-COMBINING SUBSYSTEMS

The light received at each collector telescope is relayed to a central station that contains the beam-combiner and signal-detection systems. The purpose of the beam combiner is to coherently interfere the wavefronts that have been collected by each of the apertures. The current baseline configuration for the beam combiner will be described by its component subsystems. The most demanding subsystems exploit technology that will be developed for the Keck Interferometer, Space Interferometry Mission (SIM), and Space Technology 3 (ST-3) (formerly DS3) as described in Chapter 12. These subsystems are required whether the interferometer is configured for planet detection or aperture synthesis imaging. A functional block diagram of the beam-combiner system, operating in nulling mode and organized as a set of functional subsystems, is presented in Figure 11.3. The subsystems for cophasing, beam interference, and fringe detection are shown.

Cophasing Subsystem. The cophasing subsystem intercepts light beams from the collector telescopes, aligns them with the optical axis of the beam combiner, compresses them from a diameter of 15 cm to a diameter of approximately 3 cm with an afocal telescope, and cophases them prior to the beam-combining modules. If the beams require wavefront compensation, this would be done with a deformable primary mirror or an adaptive optics system located after the beam compression.

A pair of beam steering mirrors direct each beam, relayed from a collector telescope, into the combiner spacecraft and align it with the beam-combiner optical axis to sub-arcsecond precision. This alignment ensures that the interfering beams overlap and are parallel at the beamsplitter. A star-tracker, employing a quad-cell detector, and a

shear sensor are used to generate the tip-tilt error signals for the fast steering mirrors at each telescope and to control the beam steering mirrors. The hardware exploits mature technology that has been used in a number of ground-based interferometers and will be demonstrated in space by the SIM and ST-3 missions. Separate delay lines are required for each of the input beams. To obtain a null depth of 10^{-6} at a wavelength of 7 μm, the pathlengths must be controlled with a precision of about 3 nm (Table 10.2). The necessary dynamic range and precision are achieved by implementing an active optical delay line (ODL) with several levels of real-time control.

After the delay lines, a fraction of the near infrared light is split off from each beam by a dichroic beam-splitter and is redirected to a fringe tracker. The fringe tracker operates in the near infrared at a wavelength of 2 μm to combine the beams in pairs and measure phase fluctuations arising from variations in the optical path difference. This measurement is made by modulating the pathlength in one of any two beams within the fringe tracker using an actively controlled delay line, employing phase measurement interferometry augmented with estimates of the group delay. Error signals in path difference that are detected by the fringe tracker are used to control the delay lines external to the fringe tracker to minimize the optical path difference between the interfering beams. The two beams that contain the science signal are not subject to the modulation introduced by the fringe tracker and continue on to the nulling or imaging subsystems. Laser metrology gauges are used to monitor internal path lengths and correct for offsets between fringe positions measured by the cophasing and nulling/imaging subsystems.

Nulling and Imaging Subsystems. After the input beams have been conditioned so that they are parallel and cophased, they are then passed to a beam-combining module, where the beams are interfered, spatially filtered, and detected. Different modules or modes of a sin-

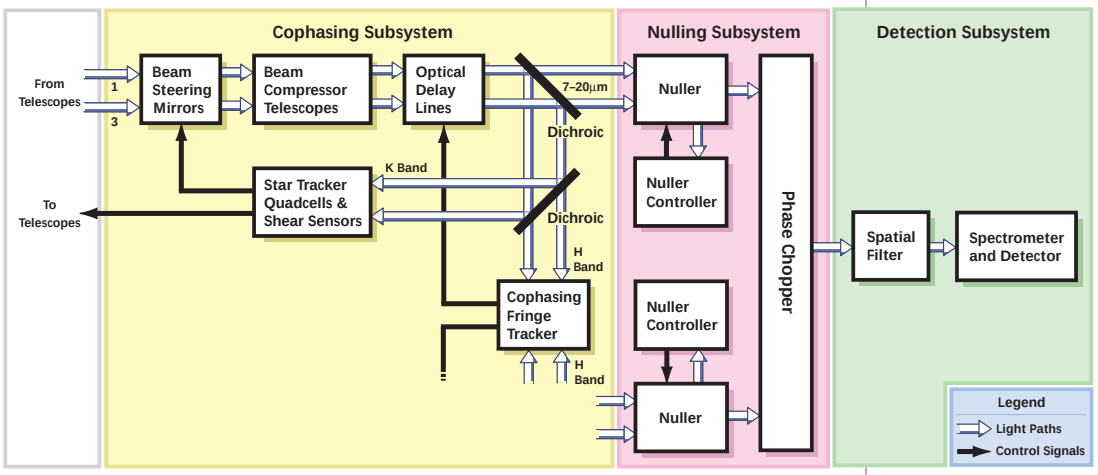

Figure 11.3. Beam combiner layout.

gle module allow the beams to be combined in a different manner for either planet detection or synthesis imaging.

Nulling Beam Combiner. For planet detection, a nulling beam combiner must introduce an achromatic, 180° phase shift between its two input beams so that the on-axis light from the star can be destructively interfered. A conventional beam-splitter by itself would be unsuitable as a nulling combiner, because it introduces only a 90° phase shift of one beam relative to the other. To achieve the necessary null depth, we require an achromatic phase shift of 180 ± 0.08° across the short wavelength part of the 7-20 μm band. At least two different nulling architectures are capable of providing the necessary phase shift. The final choice of architecture will be determined by experience acquired from nulling experiments in the laboratory and with the Keck Interferometer, Large Binocular Telescope (LBT), and SIM.

The first architecture produces an achromatic phase shift using a beamsplitter with specially designed dielectric waveplates inserted in one of the two input beams. Preliminary work indicates that bandwidths of $\Delta\lambda/\lambda \sim 0.5$ are thereby possible in the 7-20 μm band, and that two sub-bands would probably be required to span the whole wavelength range (Burge unpublished). These sub-bands would be further subdivided to enable R~20 low-resolution spectroscopy needed for planet characterization. The transmission-to-reflection ratio of the beamsplitter must be matched to within ±0.25% for the shorter wavelengths. Multi-pass beam-combiners that balance transmission and reflection are now being studied.

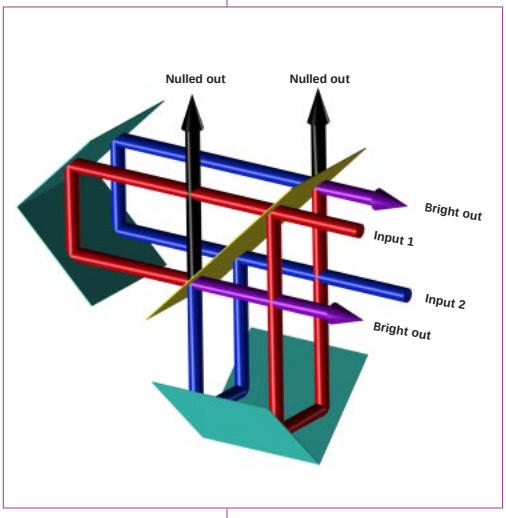

Figure 11.4. Nulling beam combiner with rooftop prisms.

The second approach uses a polarization flip of the beams to produce the null. The direction of the electric field vectors in the two beams is rotated by 180° with respect to each other, using either crossed roof-prisms or cat's-eye mirrors. These elements are arranged so that the interfering beams make a double pass (once in transmission and once in reflection) through the beamsplitter where the beams are interfered. The arrangement employing the rooftop prisms is shown in Figure 11.4. Although this type of combiner results in a more complicated optical train, the requirements on the beamsplitter are very much relaxed. This results from the fact that the beamsplitter is used in double-pass, which explicitly guarantees that it will not alter the transmission-to-reflection ratio of the interfering beams.

For planet detection with chopping, a second stage of beam combination is employed to null the first sidelobe on one side of the central

null in the interferometer beam pattern, as shown in Figure 11.5. Nulling of the sidelobe is achieved by introducing ±90º phase shifts between the two nulled beams produced by the first stage of beam combination. This phase offset need not be achromatic and could be introduced with a single-pass beam combiner by pistoning one of the delay lines in the second stage by an appropriate amount.

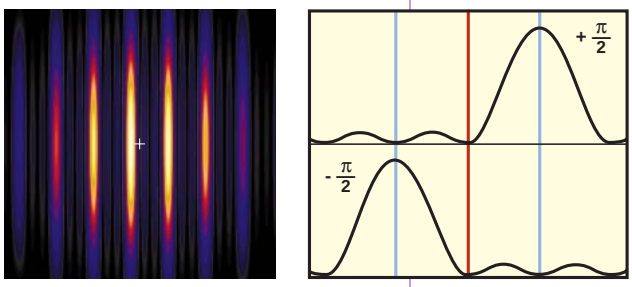

Figure 11.5. The transmission pattern on the sky for both chop orientations of the dual Bracewell configuration.

Imaging Beam Combiner. Although planet detection has been stressed in the description of the interferometer, TPF will also be capable of aperture-synthesis imaging using a separate beam-combiner module. The array is used to sample the Fourier transform of the brightness distribution of a source, where each sample comprises measurements of fringe phase and calibrated fringe visibility. Each measurement represents source structure at a single spatial frequency determined by the separation and vector orientation of the collectors relative to the source. To produce a high-fidelity image, the collectors must change their separations and orientations to sample the spatial frequencies present in the source structure.

In contrast to ground-based interferometers, which are subject to phase errors introduced by atmospheric turbulence, space-based interferometers such as SIM and TPF are designed to be phase-stable. They are able to use an unresolved object to provide a phase reference to link the individual complex visibility measurements, which obviates the need for measuring closure phases. This reference source may be separate from the target object or may be its compact core (observed in a waveband outside the science bandpass). The cophasing system should therefore be able to point away from the boresight, if necessary, to track fringes from the phase reference source. This approach is identical in concept to that currently employed for dual-star astrometry at Palomar Testbed Interferometer (PTI) and which will be implemented at the Keck Interferometer. The imaging beam combiner is functionally simpler than the nulling combiner, and can be designed to allow simultaneous fringe measurements on the six baselines provided by the four telescopes.

Detection Subsystem. The detection subsystem spatially filters the fringe, disperses it, and images the dispersed fringe onto a cooled multi-pixel detector. Although it is described here as a separate unit, its function may be partially integrated with the nulling or imaging beam-combiners.

Spatially filtering the combined beams serves to preferentially pass the on-axis and aberration-free component of the interfering wave-

fronts, removing aberrations that would degrade the depth of the null. Simulations have shown that a null-depth of 10^{-6} or better can be obtained with a spatial filter restricted to 0.6 of the Airy-disk diameter (Ollivier and Mariotti, 1997). Spatial filters may be implemented using single-mode fiber optics, feed horn waveguides, or pinholes. Fibers or waveguides are preferred because they place looser requirements on beam pointing.

After spatial filtering, the light is re-collimated and dispersed by a spectrometer to yield 20 or more spectral channels in the science band. Dispersing the light has advantages for both imaging and planetary detection. If the source structure is known to be essentially independent of wavelength, the multi-wavelength measurements provide simultaneous samples at numerous spatial frequencies. Dispersing the combined light is particularly important for planet detection; the separation of the fringes on the sky is wavelength-dependent, and therefore fringes measured over a narrow bandwidth have a higher contrast.

OPERATIONS DURING OBSERVATIONS

Planet detection will be accomplished by rotating the interferometer with a fixed baseline length, optimized according to Figure 7.4 for each target star. The system will complete a 360° rotation every 8 hours, providing for up to three full revolutions on a single star each day (one star/day). The spacecraft will travel along a polygonal path, approximating a circle as shown in Figure 11.6a. Data collection will

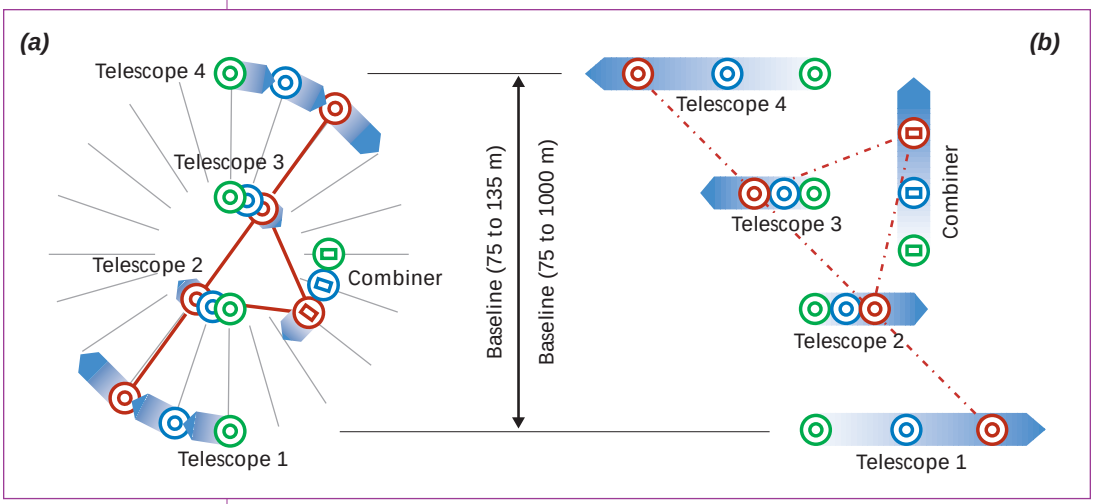

Figure 11.6. Flight paths during data acquisition for (a) planet detection and (b) imaging. Three successive positions are shown for each mode (green, blue, red), with arrows indicating straight line flight paths.

occur while drifting along the sides of the polygon, with maneuvers occurring at the corners of the polygon. For spectroscopy in the nulling mode, the observation pattern is the same but with substantially longer integration times determined by the desired spectrometer resolution. The rotation rate of the formation can be decreased during these observations to conserve propellant.

Imaging is done by a shear-drift maneuver as shown in Figure 11.6b. An initial baseline is established, and the spacecraft are allowed to drift along straight lines while tracking interferometric fringes. Data are taken continuously during the drift, which is allowed to progress until a maximum baseline (~1000 m) is established. Thrusters firing may cause momentary breaks in the data acquisition while disturbances settle. Changes of direction occur when the outer collectors reach the ends of the required baseline. Due to the long distances traversed and the desire for rapid motion to traverse these distances, fuel demands for this mission phase are the most severe. Other possibilities for maneuvering during the imaging mode do exist, including two-dimensional arrays with the four collectors arrayed in a circle. This would enable more non-redundant baselines to be measured simultaneously, but preliminary estimates suggest that covering the *uv*-plane with a two-dimensional array may require more maneuvers and thus use more propellant and time.

SPACECRAFT SYSTEM CONFIGURATION AND DESIGN

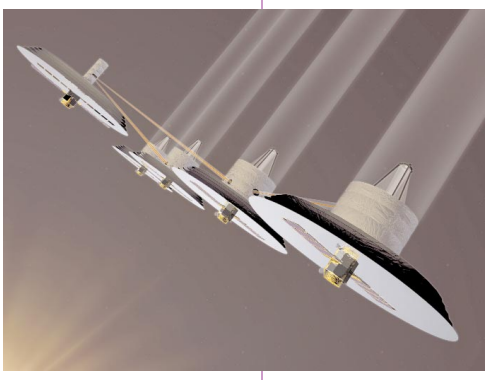

Figure 11.7. Artist's rendering of TPF reference design. The spacecraft are shown to scale with a slightly shortened baseline. Infrared (semi-transparent) and metrology (orange) beams are shown for illustrative purposes.

An artist's rendering of the TPF formation is shown in Figure 11.7, with details of the individual collector and combiner spacecraft concepts developed for this study shown in Figure 11.8. A thermal shield, penetrated by a low thermal-conductivity supporting structure, separates the spacecraft bus and optical elements, with nominal spacecraft temperatures of 300 K and optics temperatures of 35 K. The cryogenic instruments are shaded from solar and other vehicle-emitted infrared energy, including that from its neighbors. The spacecraft bus is on the sun-lit side of the thermal shield, providing power to the instruments as well as coarse attitude reference and control, navigation, and communications. The thermal shield design shown permits offset pointing up to ±45 degrees about the anti-sun line. The allowable rotation can be increased by increasing the sunshield diameter, with constraints imposed primarily by the desired minimum baseline.

Mass and power summaries are provided in Table 11.3. Mass assumptions are based on existing spacecraft designs. Electric propulsion is assumed, as is advanced avionics packaging, with weight and power savings consistent with systems currently under development at JPL and elsewhere. Also assumed are Li-ion batteries, a technology already in use for terrestrial commercial applications and undergoing scale-up and space development for near-term flight applications.

The autonomous formation flying system (AFF) handles inter-spacecraft communication after deployment. The spacecraft features a stellar inertial attitude reference system, which provides adequate

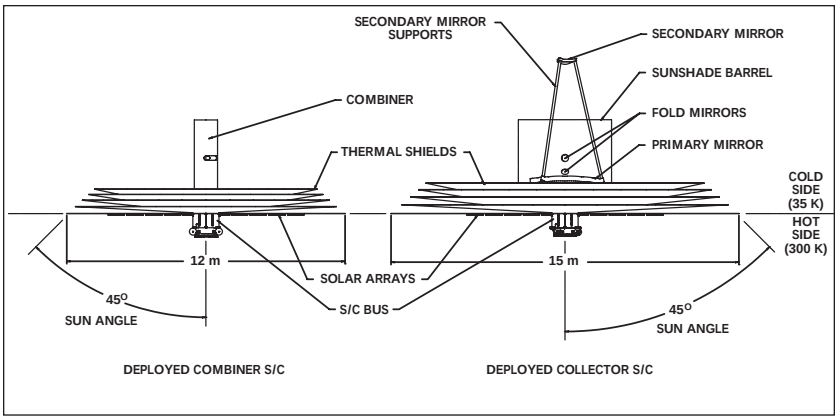

Figure 11.8. Spacecraft detail of the illustrative design concept as show on the previous page.

pointing for fringe acquisition by the interferometer. Reaction wheels, with vibration isolation using Chandra derivative techniques, are used for momentum accumulation and slewing. Wheel unloading is via thrusters, which are also used for maneuvering and precision navigation control. Structural vibration isolation, either active or passive, is also under consideration, but will require detailed structural modeling beyond the scope of this study. Thrusters are mounted to minimize plume impingement upon the thermal shield; wheels and thruster modulation are utilized to correct for residual effects. System-specific analysis of plume impingement effects is required in future studies.

Figure 11.9 shows the propellant requirement as a function of rotation period for planet finding mode. Propulsion requirements in this mode are kept small by the choice of an 8-hour rotation period. The large number of maneuvers in imaging mode, the moderate acceleration requirement (~0.1 N) in both modes, and low impulse required for fine positioning (±5 cm) and velocity control drive the propellant mass. These requirements are best met with higher-thrust electric propulsion (EP) options (I_{sp}>1000 s). Options include Hall effect thrusters (HETs) and high-power pulsed-plasma thrusters (PPTs). Chemical propulsion (mini-hydrazine, hot gas, or heated hydrogen) is also under consideration, but initial results indicate significantly larger fuel loads, particularly for imaging mode observations. Maximum drift velocities (limited by interferometer capabilities) can be achieved rapidly, within the first 2 to 6 m of total motion, using 0.1 N thrusters. Lower-thrust options would force a significant reduction in the time spent in imaging mode. HETs require approximately 1400 W during operation, with a maximum operational duration approximately 5 minutes/maneuver. Although significant, this power requirement is readily achievable and does not warrant the addition of chemical propulsion. A small amount of additional fuel will be required for reaction wheel momentum unloading, thruster off-modulation, differential solar acceleration, and other aspects of formation flying.

The full Sun exposure provided by the heliocentric orbit simplifies the

Table 11.3. Mass and Power Summaries

	Mass (kg)	Mass Cont. (kg)	Total Mass Cont. (kg)	Avg. Power (W)	Avg. Power Cont. (W)	Avg. Total Power (W)
Combiner						
Combiner Optics (includes cryo-coolers)	200	60	260	500	150	650
Struct. and Mech.	151	23	174	-	-	-
Thermal	98	14	112	22	6	27
Power	67	10	77	23	3	26
Attitude Cntrl.	34	5	38	80	12	91
Comm. and Data Mgmt.	18	3	21	62	9	71
Propulsion	96	15	111	300	60	360
Propellant	23	5	28	-	-	-
Spacecraft Total	487	74	561	486	90	576
Combiner Total	687	134	821	986	240	1226
Outer Collector (x 2)						
Collector Optics	200	60	261	102	31	133
Struct. and Mech.	146	21	167	-	-	-
Thermal	144	21	165	22	6	27
Power	66	10	76	22	3	26
Attitude Cntrl.	34	5	39	80	12	91
Comm. and Data Mgmt.	10	1	12	42	6	48
Propulsion	96	15	111	300	60	360
Propellant	35	7	42	-	-	-
Spacecraft Total	531	81	611	466	87	553
Outer Collector Total	731	141	873	568	117	685
Inner Collector (x 2)						
Collector Optics	200	60	261	102	31	133
Struct. and Mech.	146	21	167	-	-	-
Thermal	144	21	165	22	6	27
Power	66	10	76	22	3	26
Attitude Cntrl.	34	5	39	80	12	91
Comm. and Data Mgmt.	10	1	12	42	6	48
Propulsion	96	15	111	300	60	360
Propellant	17	4	21	-	-	-
Spacecraft Total	513	77	590	466	87	553
Inner Collector Total	713	137	851	568	117	685
Launch Adapter Struct.	450	50	500			
Total (5 spacecraft)			4769			3967
LV Capability			6100			
LV Margin			1331			

power subsystem design. Nominal and limited amounts of battery recharge power are provided by fixed solar arrays; due to the relatively narrow Sun-angle range, solar array gimballing is not required. Batteries meet burst-mode operational power requirements for the HET thrusters, with a 17% duty cycle corresponding to 10 minutes of

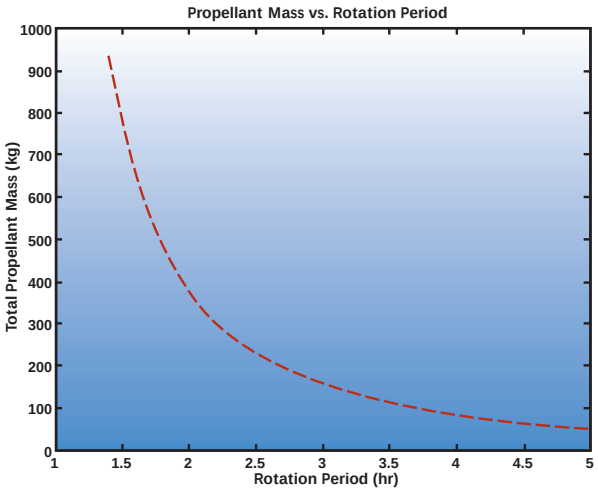

Figure 11.9. Illustrative dependence of the propellant mass on rotation period. This figure shows the total mass that would be required for planet observations over the mission lifetime for a similar system described in Stephenson (1998).

operation per hour. Battery power is also available for the initial phases of transfer orbit and in case of non-nominal operation.

Assuming TPF will collect data for 24 hours/day at an average rate of 24 kbps, just over 2 Mb of data will be generated per day. An optical communications band at 400 kbps can downlink a single day's data to the 34 m deep space network (DSN) stations in less than two hours, and storage for approximately 7 days' data will be available onboard the spacecraft. These data storage and communications requirements can be satisfied with existing technology.

PASSIVE COOLING AND THERMAL DESIGN

The thermal design for a free-flyer TPF spacecraft is dominated by the requirement that all optical components be at less than 40 K. The presence of neighboring spacecraft within the fields-of-view of the cold optics and the necessity to accommodate line-of-sight pointing anywhere within a 60° half-angle cone (±15° depending on design trades) about the anti-sun line place further requirements on the thermal design. Both L2 and Earth-trailing orbits provide the large field of view to cold space necessary to make passive cooling below 40 K possible.

Passive cooling to 33 K has already been demonstrated by Wright (1980) with a 9 m^2, 3-stage radiator designed to operate in geosynchronous Earth orbit. Missions presently under development (SIRTF and NGST) also require passive cooling to <40 K and will have flown before TPF construction begins, providing further flight experience.

Passive cooling technology and design tools have advanced substantially since the development of the Wright radiator. The TPF optics cooling system will use v-groove thermal shields that radiate energy to space much more effectively than the multi-layer insulation (MLI) used by Wright. The shield surfaces will be specular, low-emittance materials (such as polished aluminum) and are arrayed with respect to each other such that they are out of parallel by a few degrees, with the 'v' opening directed to cold space. Thus, energy emitted from either shield is rejected to space after a few bounces. The result is extremely efficient radiative isolation, with effective emittance on the order of 10^{-3}-10^{-4} depending on the temperature of the shields.

There are a number of possible configurations for the TPF cold optics shields. One such configuration, which has been modeled and will meet the TPF requirements, is shown in Figure 11.10. The warm

spacecraft is isolated from the cold optics assembly by an array of eight conical specular v-groove shields. The outer set of larger diameter shields is shaped to direct the emitted energy away from the cold sections of the neighboring spacecraft. The inner shields with the same diameter as the spacecraft bus are rigid and conductive, since they are required to intercept and radiate to space the heat loads conducted through supporting structure and wiring. The outer shields are inflation-deployed and can be relatively non-conductive parallel to their surfaces.

The cold optics assembly is enclosed within a thermally conductive housing that has a specular and low-emittance exterior. The housing may be deployable, but it must also be thermally conductive in order to effectively remove heat from the cold optics and radiate it to space without developing significant internal gradients that would degrade its emissive power. The inner cylindrical surface is coated with a high-emittance material to maximize the radiative coupling from the cold optics assembly to cold space. The back of the primary mirror has a high-emittance to radiatively couple it to the interior of the cold optics housing.

TPF FORMATION FLYING

The large thermal shields and the short interferometer baselines place challenging constraints on formation-flying systems. Spacecraft shield-to-shield separations of ~10 meters and control sensitivities on the order of a millimeter are required. The formation-flying technology is already in development for ST-3, as described in Chapter 12, but distributed real-time fault-protection systems to prevent collisions in case of unexpected failures will require TPF-specific development. The presence of the neighboring spacecraft will also affect thermal design and contamination control, as described elsewhere in this

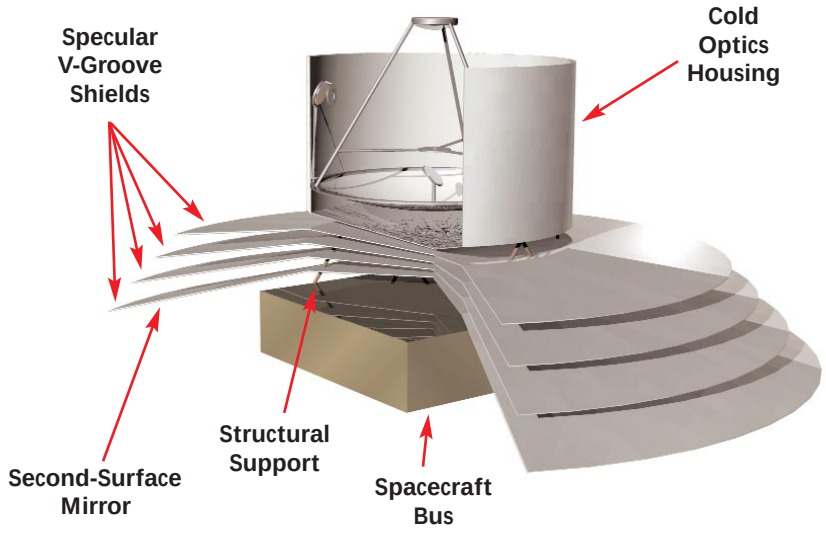

Figure 11.10. Schematic of overall thermal control configuration.

chapter. The overall system architecture for the formation-flying systems is described below.

The TPF formation is shown schematically in Figure 11.11. A distributed sensing-and-control AFF approach is used to enable a virtual-truss rigidity of the separated spacecraft that maintains the tight tolerances on overall planarity and alignment for the interferometer dynamic range. Relative measurements between neighboring collectors and combiners are depicted. Range, range rate, azimuth, and elevation data are obtained and processed at a low frequency (~1 Hz), both locally on each collector and globally by the combiner that also functions as the formation navigator and the command, control, and communications executive. This distribution of sensing, decision, and control action functions at the local collector level and the global combiner level may be the optimum division of autonomous management functions for TPF and future larger formations.

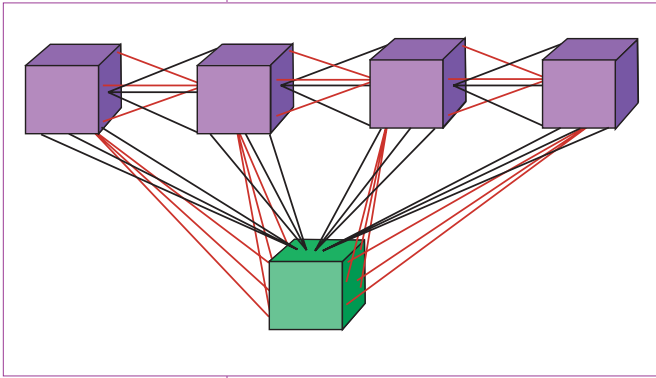

Figure 11.11. TPF formation control and communications schematic. Relative measurements between spacecraft are indicated by lines.

The basic functions of the AFF system for the TPF constellation are:

- Initial formation acquisition of the separated spacecraft using relative 3-D position sensing by the AFF radio frequency (RF) receiver/transmitter on each spacecraft.
- Provision of relative range, range rate, and azimuth/elevation bearings between spacecraft over the full range of inter-spacecraft separations (10 to 1000 m) for coordinated maneuver control.
- Determination of relative position knowledge to ±1 cm, relative velocity to ±0.1 mm/s, and attitude knowledge to ±1 arcmin.
- Six degree-of-freedom attitude and translation control of each spacecraft, using bi-directional arrays of micro-thrusters and vibration-free magnetic-bearing reaction wheels.

The AFF system handles spacecraft-to-spacecraft communications after deployment and enables determination of relative attitudes of the spacecraft in the formation. The relative position of each spacecraft in the ensemble can be precisely determined from the spacecraft-to-spacecraft phase and range data. Because the transmission and reception of the dual one-way range and phase observables are nearly

simultaneous, there will not be a stringent requirement for a stable clock.

Changes in relative positions and orientations of the multiple spacecraft will be sensed automatically by the onboard control systems that initiate corrective maneuvers to maintain the formation geometry.

CONTAMINATION

Mission lifetime and passive cooling considerations are expected to lead to strict, but achievable, cleanliness requirements for the thermal radiator surfaces of the spacecraft. It is expected, and will be tested experimentally, that the optics will be relatively insensitive to contaminant layers that are much less than a wavelength thick. The remoteness of the optics from the thrusters, along with baffling, can limit contamination to acceptable levels. Potential sources of contamination for TPF include propulsion by-products and outgassing of spacecraft components. Transport analysis of propulsion plumes can limit contamination and prevent noise signals from thermal emission by particles that might otherwise enter the telescope fields of view (Simpson and Witteborn 1977).

A variety of contaminant species from outgassing of spacecraft components and propulsion-system exhaust, including water vapor, will condense onto thermal and optical surfaces at 35 to 40 K. Ice from the water vapor has several absorption peaks in the infrared and can increase the emissivity of thermal radiators. The increased emissivity will result in a temperature rise for the surface, decreasing the efficiency of active coolers used to cool the focal plane, which rely on precooling from the passive radiators. Figure 11.12 shows the predicted decrease in reflectance (and resulting increase in emissivity) with increasing ice cryolayer thickness for an optical surface coated with gold at a wavelength of 10 microns. This figure also shows measured values of the emissivity for a stainless steel surface. The thermal design described earlier has been modeled with degraded emissivities, and will meet system requirements with a 50% degradation of the emissivity of thermal radiator surfaces, corresponding to a 0.4 μm-thick ice layer. Further optimization of the thermal design in conjunction with contamination analysis can keep contamination within this limit.

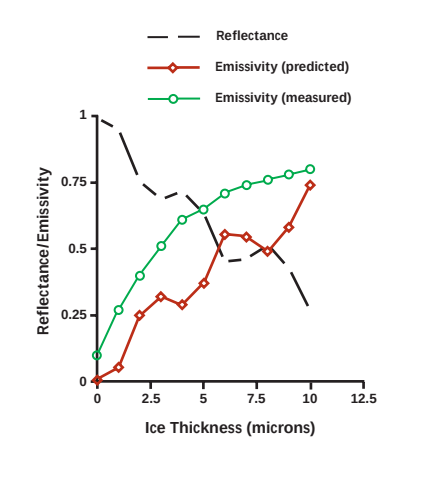

Figure 11.12. Degradation of thermal surfaces and optics due to contamination by ice (modeled at 10 μm).

Optical surfaces at 35 to 40 K will be out of the direct path of propellant contamination, but may be susceptible to scattered contamination from propellant plumes. Typically, 99% of the thruster plume mass-flux is within an angle of 90°. The use of non-contaminating (e.g. cold gas or high-temperature hydrogen (Westerman and Miles 1998)) thrusters in certain areas when operating with short baselines, com-

bined with specifically designed plume shields can be used to prevent contaminants from reaching the optics. Model predictions indicate that an ice layer build up of 0.60 μm thickness will degrade reflectance at 10 μm by no more than 1%. Amplitude matching at the beam combiner will compensate for such variations in the signal from the individual collectors as described earlier.

INTEGRATION AND TEST

In the previous round of industry studies, all three contractors identified I&T as the most formidable aspect of the TPF mission. All of the possible TPF configurations are very large, with optical systems that must deliver extremely high performance at cryogenic temperatures. As described in Chapter 12, most of the technologies required will have been demonstrated in flight missions before TPF is built. Nonetheless, the complete TPF system must be integrated and have its performance verified prior to launch.

Testing of an optical system distributed on several spacecraft flying in formation offers particular challenges. The system must be shown to achieve the required performance without all spacecraft systems in full operation. The I&T approach for the TPF instrument combines full performance testing of major subsystems with an integrated system performance test over a limited range of operating conditions. The instrument, spacecraft attitude control system, and instrument-spacecraft control interaction ground tests verify all factors relevant to mission performance.

The major optical subsystems, consisting of the collector telescopes with relay optics and the combiner, are first tested individually, using high-fidelity light sources and measurement equipment, to verify control systems and to determine beam characteristics (rms wavefront errors, amplitude uniformity, polarization, scattered light) important in producing a dark null for planet detection. Some of the test apparatus needed for subsystem characterization will be based on the TPF technology testbed program, designed to verify performance of key components. TPF testbeds will be used to analyze such components as lightweight primary mirrors, relay optics control, beam conditioning optics (control of overlap, wavefront tilt, and aberrations), and nulling beam combiners.
The integrated system test will require a simulation of free-flyer operation in a 1 g environment. Simulation of disturbances to the relative spacecraft positions and to optical beams will be used to check operation under expected conditions on orbit. Spacecraft modeling will play a key role in predicting disturbance levels and how such disturbances can be included in the integrated test. Characterizing system performance as a function of disturbance levels will give confidence in expected on-orbit performance and will provide a database for use in instrument maintenance.

The interferometer will be tested in a simulated on-orbit environment

(including temperature and vibration disturbances as shown in Figure 11.13). The figure shows a preliminary TPF concept in an existing thermal vacuum chamber that is presently undergoing conversion to liquid helium operation for other projects. During the thermal vacuum testing the mirrors are maintained in cryogenic conditions while the spacecraft bus is held at its on-orbit temperature.

The integrated testing shown schematically in Figure 11.14 provides a full interferometric demonstration of end-to-end TPF system performance in varied conditions. A collimated wavefront representing starlight enters each collector and is relayed to the combiner. Preliminary subsystem tests measure features of the compressed output beams (stability, position, quality, etc.). Combiner subsystem testing uses simulated input beams to demonstrate combiner nulling and signal extraction capabilities for planet detection and astrophysical imaging.

Experience and resources from precursor projects such as ST-3, SIM, and NGST will be applied to TPF integration and test. For example, ST-3 will demonstrate techniques for separated spacecraft interferometry as well as precision autonomous formation flying and developing the requisite testing protocols. SIM will demonstrate distance gauging

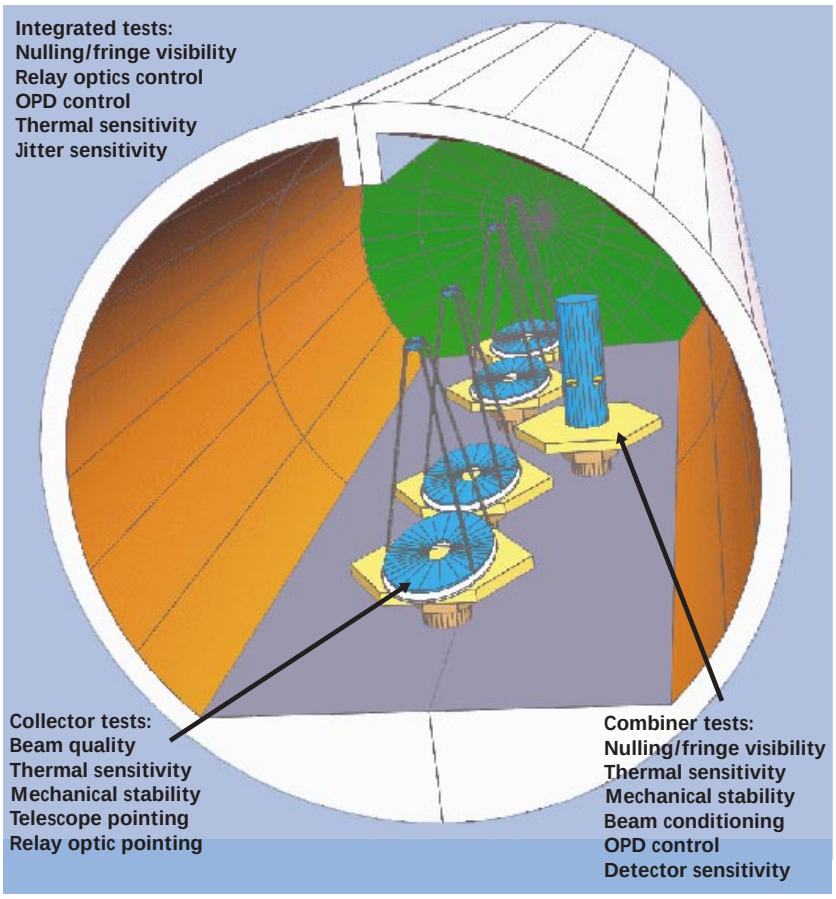

Figure 11.13. TPF separated spacecraft concept with 4 m x 2 m elliptical mirrors shown in an existing thermal vacuum chamber.

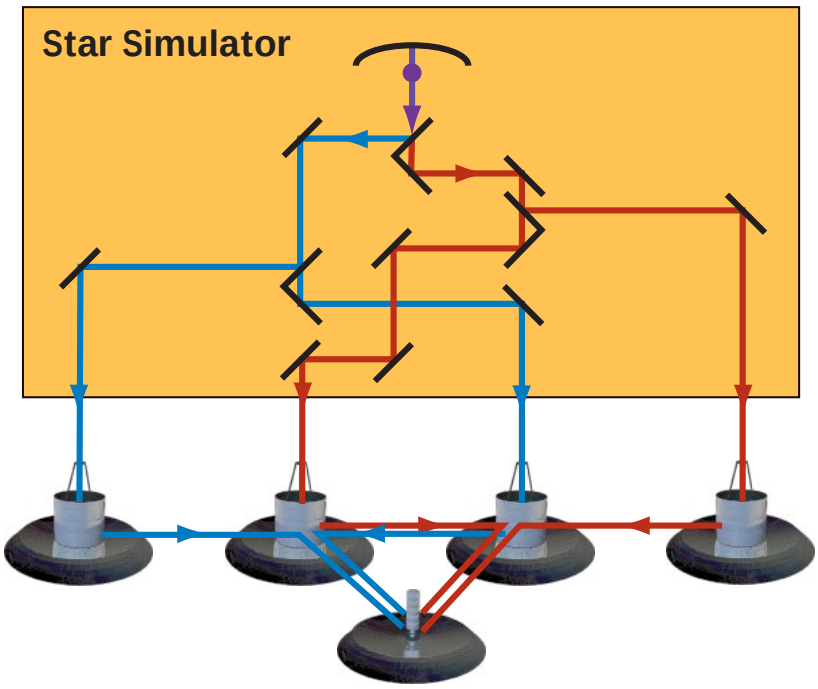

Figure 11.14. Schematic of integrated system performance in vacuum chamber using simulated starlight to provide a co-phased, collimated wavefront entering all collectors.

and pathlength control, precision nulling, vibration suppression techniques, deployable structures, integrated modeling, and the integration and test of large missions. NGST will demonstrate the integration and test of technologies such as large-aperture and deployable optics, precision cryogenic optical systems (including actuators and active wavefront correctors), advanced infrared focal planes, and autonomous operations. The planning for development of major TPF technologies is described in greater detail in Chapter 12.

ORBIT TRADES: L2 VS. EARTH-TRAILING

Two different trajectory options are presently under consideration for TPF. The first, and presently better understood, is an Earth-trailing trajectory with a C_3 of 0.4 km^2/s^2, similar to the one used by the SIRTF mission (Figure 11.15a). The second is a quasi-halo orbit (Gomez *et al.* 1997, Barden and Howell 1998) near the Sun-Earth L2 libration point with a C_3 of –0.69 km^2/s^2 (see Figure 11.15b). Figure 11.15c shows a typical TPF formation zooming in on a segment of the quasi-halo orbit. The figures are shown in Sun-Earth rotating coordinates. A variant of the second, which uses a lunar swingby to reach the halo orbit, requires a slightly smaller C_3 of –2.24 km^2/s^2.

Several factors must be considered in the selection of the nominal trajectory. First, the Earth-trailing option is feasible with current technology, whereas a significant feasibility study is required to evaluate the L2 option and the requisite astrodynamic technology. However, L2 offers several significant advantages that merit consideration. The

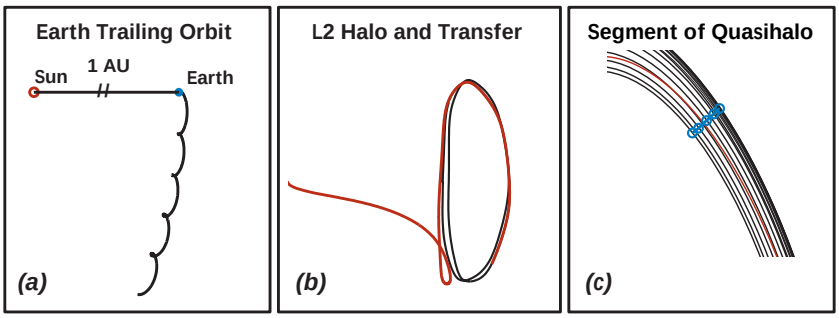

Figure 11.15. Trajectory options for TPF.

chief advantage is that additional (possibly replacement) spacecraft could be launched into the formation at any time throughout the mission. This enables a much more flexible launch strategy, which is not feasible with the Earth-trailing orbit. This capability not only lends itself to catastrophic-error recovery scenarios (i.e. replacing the loss of a spacecraft), but also to extended mission scenarios, since spacecraft could be incrementally replaced as they near their end-of-life.

The L2 option requires a more complex control algorithm for formation flying, but the propellant required to maintain the formation at that orbit may be less than that required for the Earth-trailing option. Due to the instability of the L2 region, great flexibility in the control of the formation is possible, since very small maneuvers can significantly change the characteristics of the trajectory. Furthermore, L2 provides a larger payload capability, since the energy required to launch into the L2 orbit is less than that for the Earth-trailing trajectory. The Earth-spacecraft communication distance for a spacecraft at L2 is never more than approximately 0.01 AU from the Earth, whereas the communication distance for the drift-away option can be more than 0.6 AU by the end of the mission. In addition, at L2, both the Sun and Earth are always behind the spacecraft. Thus, observation planning and mission operations are much less complex at L2 than in the Earth-trailing. However, the necessary control algorithms have not yet been developed.

LAUNCH VEHICLE PACKING AND SYSTEM DEPLOYMENT

The launch strategy for TPF depends on the trajectory option. As described earlier, the baseline Earth-trailing orbit requires all spacecraft to be launched at once to achieve the formation. Separate launches would require rendezvous maneuvers that can be prohibitive since the spacecraft in the Earth-trailing orbit are constantly drifting away from the Earth. The L2 halo orbit can accommodate several launch opportunities yearly. Hence the spacecraft might be launched into an L2 halo orbit at different times using smaller launch vehicles.

Table 11.4 summarizes the payload capabilities of various launch vehicles. The total mass of the TPF spacecraft system is estimated at 4,000 to 5,000 kg. Thus for Earth-trailing, the Extended Expendable Launch Vehicle (EELV), Ariane 5, and VentureStar are the only

launch vehicles capable of sending TPF into the drift-away orbit. By contrast, since the individual spacecraft masses are less than 1000 kg, many more launch vehicle options are open to the L2 halo-orbit option with its more flexible launch strategy. An example launch and deployment sequence is shown in Figure 11.16.

Recent launch vehicle development will result in many options for the TPF mission. The EELV development and the VentureStar Reusable Launch Vehicle (RLV) will both be fully mature systems by the time of the TPF launch. All variants of the EELV (commercial and military) are scheduled to be fully operational by the end of 2002. The RLV is scheduled to be operational by 2005 with the X33 prototype flying in 1999. The United States Air Force has recently issued contracts for the first buy of EELV launchers. The rough estimated cost for the heavy variants of the EELV should be between $150M to $200M as

Table 11.4. Launch Vehicles

	Candidate Orbits		
	Lunar Swingby to L2	L2 Direct	Drift Away
	C_3 Energy (km^2/s^2)		
	(-2.24)	(-0.69)	(0.40)
Candidate Launch Vehicle	**Maximum Payload Mass (kg)**		
Arianespace			
Ariane 5	4998	4855	4617
Boeing			
Delta III	2835	2754	2650
(EELV) Delta IV Heavy	TBD	TBD	TBD
(EELV) Delta IV Medium (0 SRMs)	TBD	TBD	TBD
(EELV) Delta IV Medium (w/SRMs)	TBD	TBD	TBD
Lockheed Martin			
Proton M Breeze M	4410	4284	4074
Atlas IIIB	3808	3213	3056
(EELV) MLV A	3859	3749	3565
(EELV) MLV G (0 SRMs)	3381	3284	3123
(EELV) MLV G (5 SRMs)	5807	5641	5364
(EELV) HLV-G	11,800(TBR)	11,500(TBR)	10,900(TBR)
VentureStar RLV	6600(TBR)	6400(TBR)	6100(TBR)

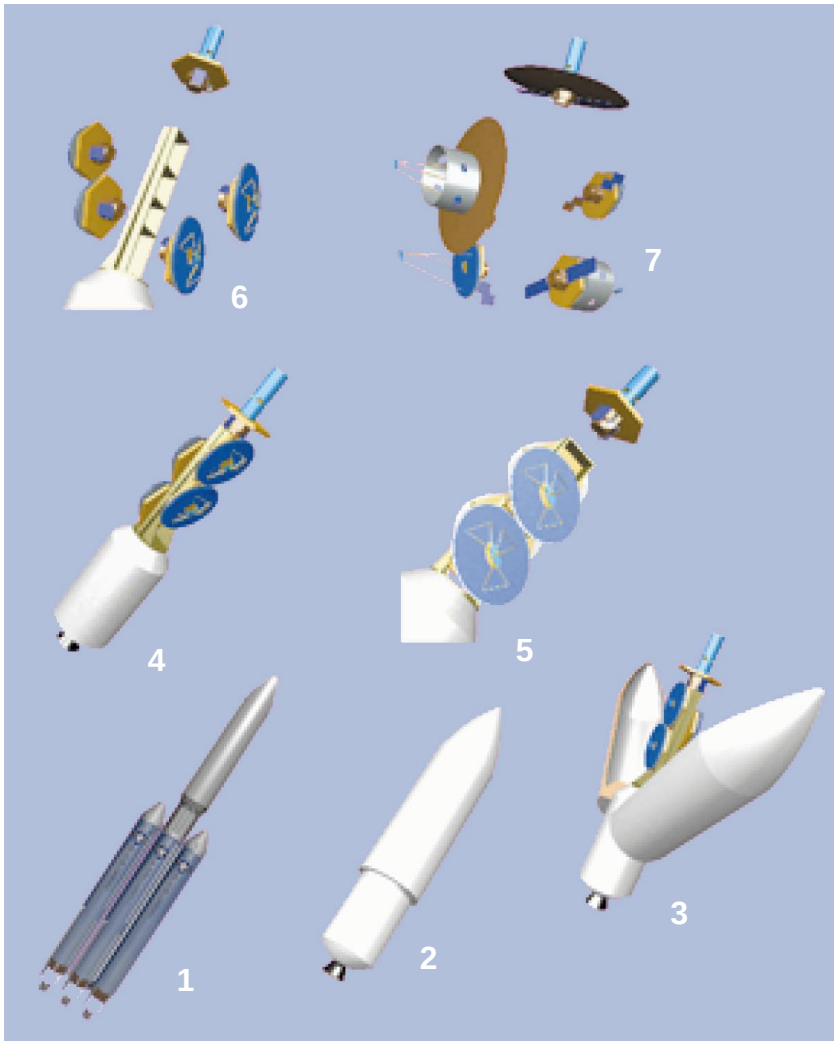

Figure 11.16. The launch and deployment sequence of a TPF concept with 4 m x 3 m primary mirrors showing an EELV launch vehicle.

compared to the Titan IVB for $450M. This will give the TPF mission a wide range of cost-effective launch solutions. Figure 11.17 shows the EELV/Ariane 5 and RLV payload volumes with examples of packing arrangements that could be used for a TPF mission.

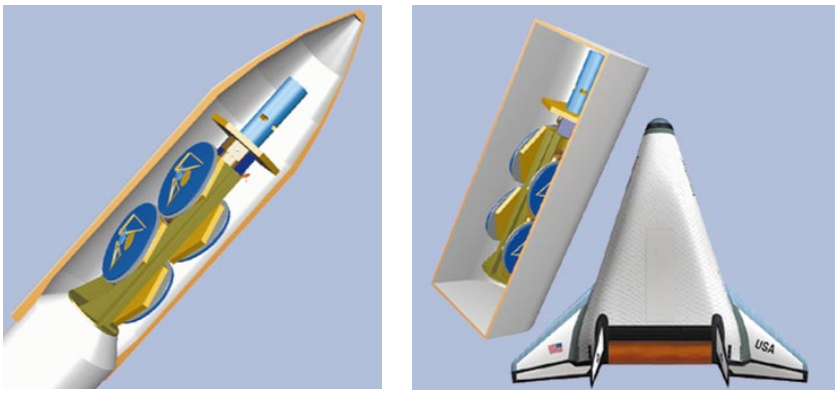

Figure 11.17. Fairing and Payload Module Options: EELV (HLV-G) or Ariane fairing (left) and VentureStar RLV (right).

REFERENCES

A Road Map for the Exploration of Neighboring Planetary Systems (ExNPS) 1996, edited by C. A. Beichman (Jet Propulsion Laboratory: Pasadena, CA), JPL 96-22.

Barden, B.T. and Howell, K.C. 1998, in Proc. *AAS/AIAA Space Flight Mechanics Meeting*, Monterey, CA, 9-11 February 1998, AAS 98-169 (Univelt: San Diego, CA).

Gomez, G., Masdemont, J.J. and Simo, C. 1997, in Proc. *AAS/AIAA Space Flight Mechanics Meeting*, Huntsville, AL, 10-12 February 1997, AAS 97-106 (Univelt: San Diego, CA).

Ollivier, M. and Mariotti, J.M. 1997, *Appl. Opt.* **36**, 5340.

Simpson, J.P. and Witteborn, F.C. 1977, *Appl.Opt.* **16,** 2051.

Stephenson, R.L. Jr. 1998, M.S. Thesis (Massachusetts Institute of Technology: Cambrige, MA). Available from MIT as SERC #3-98.

Westerman, K.O. and Miles, B.J. 1998, in Proc. *33rd Intersociety Energy Conversion Engineering Conference*, Paper No. IECEC-98-310, held at Colorado Springs, CO, 2-6 August 1998, (Society of Automotive Engineers: Warrendale, PA).

Wright, J.P. 1980, *AIAA J.* **18**, 1512.